Internet of Things 7 (2019) 100083

Contents lists available at ScienceDirect

Internet of Things

journal homepage: www.elsevier.com/locate/iot

Research article

Enhancing the sensitivity of a chaos sensor for Internet of things

Hayder Natiq [a], M.R.K. Ariffin [a,b], M.R.M. Said [a,b,c], Santo Banerjee [a,b,*]

[a] Institute for Mathematical Research, Universiti Putra Malaysia, Serdang, Malaysia
[b] Malaysia-Italy Centre of Excellence for Mathematical Science, Universiti Putra Malaysia, Serdang, Malaysia
[c] Department of Mathematics, Universiti Putra Malaysia, Serdang, Malaysia

ARTICLE INFO

Article history:
Received 2 March 2019
Revised 2 July 2019
Accepted 3 July 2019
Available online 6 July 2019

Keywords:
Chaoticfication
Hyperchaotic behavior
Chaotic attractor
Complexity

ABSTRACT

Implementing chaotic systems in various applications such as sensors and cryptography shows that the sensitivity and complexity of these systems are highly required. Beside that, many existing chaotic systems exhibit low sensitivity, limited chaotic or hyperchaotic behavior, and low complexity, and this can give a negative effect on the chaos-based sensors applications. To address this problems, we present a cosine chaotification technique to enhance the chaotic characteristics of discrete systems. The proposed technique applies the cosine function as nonlinear transform to the output of a discrete system. As a typical example, we apply it on the classical 2D Hénon map. Performance evaluations show that the proposed technique can change the chaotic and non-chaotic states of the 2D Hénon map to the hyperchaotic state with extremely high complexity performance. Additionally, sensitivity dependence results, such as cross-correlation coefficient, number of non-divergent trajectories, and the change of complexity demonstrate that the enhanced Hénon map has higher sensitivity than the classical map. That means, the proposed technique would be very useful to enhance the employed systems in chaos-based sensors applications.

1. Inroduction

In the last four decades, chaotic behavior as a complicated nonlinear phenomenon has attracted many researchers and has been discovered in natural and man-made systems [1–3]. The nonlinear systems with chaotic behavior are rich and have several characteristics such as sensitivity to its initial conditions and parameters, unpredictability and topological mixing [4]. Thus, such nonlinear systems can be widely applied in various fields such as sensors, biomedical engineering, secure communications, and cryptographic applications [5–8]. Moreover, Chaotic models are mainly deterministic systems that generate unpredictable date series with a strong correlation to the random processes. Any chaotic system is sensitive to the initials and often produce complicated sensitivity [9]. Chaotic dynamics in classical and quantum states, can be applied to various types of sensors such as Synchronization base communication sensors [10], Quantum chaotic sensors [11], Chaos based radar and optical chaos sensors [12], and many others.

Generally, chaotic models can be sorted into two types: discrete and continuous systems. The well-known discrete chaotic models are the 1D logistic map, the 2D Hénon map [13], and the 3D Hénon map [14], whereas, the common and the

* Corresponding author at: Institute for Mathematical Research, Universiti Putra Malaysia, Serdang, Malaysia.
E-mail address: santoban@gmail.com (S. Banerjee).

https://doi.org/10.1016/j.iot.2019.100083
2542-6605/

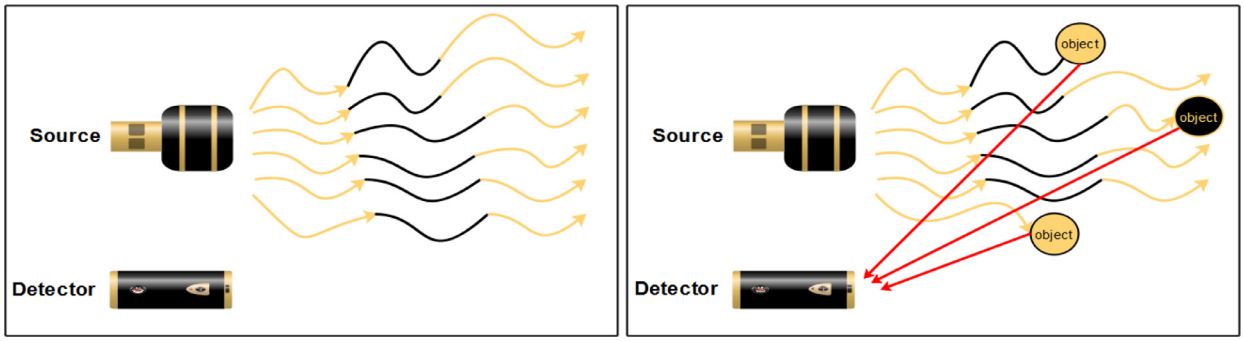

Fig. 1. Schematic diagram of the effectiveness and compatibility of a sensor signal.

most studied continuous chaotic systems are the Lorenz [15], Rössler [16], Sprott [17], and Lü [18] systems. Excluding these systems, many chaotic systems have been proposed to present different features of chaotic behavior such as enhancing the chaotic orbits of existing discrete chaotic systems [19,20], designing high dimensional discrete systems with any desired number of positive Lyapunov exponents as well as high complexity performance [21], generating new systems with self-excited attractors [22], and with hidden chaotic attractors [23].

However, applying discrete chaotic models in various aspects has shown some limitations in the performance such as weak randomness, low sensitivity and complexity [24]. In addition, most of the existing discrete chaotic systems have limited chaotic behavior, in which a small change in their parameters or even initial conditions can destroy their behaviors [25]. Therefore, many researchers have attempted to enhance the chaotic behaviors of existing discrete systems, which is known as chaotification or anti-control of chaos. In the endeavor of chaotification discrete chaotic systems, numerous systems have been improved by using nonlinear transforms to the their outputs [26–28].

Although the new discrete chaotic systems generate robust chaotic behaviors, but these systems also have performance limitations, such as using two or more existing chaotic systems to generate 1D chaotic maps, thus those have no hyperchaotic behavior, and the applied nonlinear transforms usually have complex mathematical structure. Consequently, developing a chaotification technique to enhance the chaotic characteristics including sensitivity, complexity, and randomness, can significantly encourage the research of chaos in the chaos-based practical applications.

Recently, Internet of things (IoT), which refers to uniquely identifiable things and their virtual representations in an Internet-like structure, has become a focus of research [29–31]. The major components of IoT consists of sensing, information processing, heterogeneous access, and security and privacy [32,33]. Therefore, if a chaotic system is extremely sensitive to its initial conditions and parameters, then it would be very promising for the sensors systems [5]. Moreover, a chaotic system with random-like behavior and high complexity performance, can generate excellent pseudorandom signals for security and privacy applications. It is therefore a chaotic system with aforementioned features could be very suitable for the major components of IoT.

In this paper, we propose a cosine chaotification technique to enhance the sensitivity and complexity of existing chaotic maps. As an typical example, we apply the proposed technique on the 2D Hénon map. As a result, the proposed technique could change the chaotic and non-chaotic states of the 2D Hénon map to the hyperchaotic state. Besides that, evaluation analysis results demonstrate that the proposed technique is efficient and effective for enhancing sensitivity and complexity in discrete chaotic systems.

The rest of this paper is organized as follows: In Section 2, we introduce the proposed cosine chaotification technique, and then apply it on the 2D Hénon map. In Section 3, we investigate the hyperchaotic behavior and the complexity of the new hyperchaotic map. Section 4 provides the detailed sensitivity of the new hyperchaotic map. Conclusions are presented in Section 5.

2. Enhancing the sensitivity of a chaotic sensor

In general, a sensor is a device that detects some kinds of inputs such as motion, pressure, light, or any environmental phenomena. Meanwhile, the output is a signal, which is converted to human-readable display at the detector location. However, it is very important to measure the sensitivity of the sensors. In a simple way, the sensitivity of a sensor is how much the response of the output after a small fractional changes in the input. Fig. 1 shows the schematic diagram of the effectiveness and compatibility of a sensor signal for detecting objects.

Due to the sensitivity of chaotic models to their initial conditions and parameters, chaos-based sensors have been worked effectively in the performance [5]. However, as we have mentioned, chaotic systems have some limitation that could reduce their role, especially in the IoT applications. To optimize the sensitivity of chaotic sensors, our aims are to enhance the nonlinear dynamics of chaotic systems by chaotification techniques, and then to increase the complexity performance of chaotic systems.

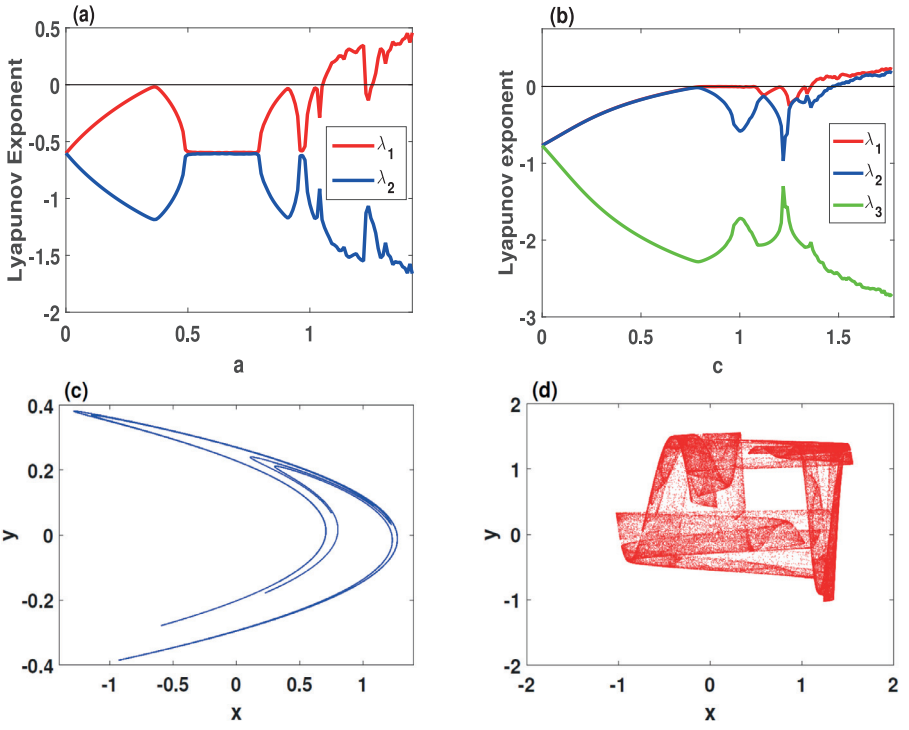

Fig. 2. Dynamics analysis of the Hénon maps for the initial values (0.1, 0.1) and (0.1, 0.1, 0.1): (a) the Lyapunov exponent of the 2D Hénon map with $a \in [0, 1.42]$ and $b = 0.3$; (b) the Lyapunov exponent of the 3D Hénon map with $c \in [0, 1.77]$ and $b = 0.1$; (c) the chaotic attractor of the 2D Hénon map with $a = 1.4$ and $b = 0.3$; (d) the chaotic attractor of the 3D Hénon map with $c = 1.5$ and $d = 0.1$.

In order to show the limitation of the existing chaotic systems, consider the 2D Hénon map [13] as our starting point, which is described by

$$\begin{cases} x_{n+1} = F_1(a, x_n, y_n) = 1 - ax_n^2 + y_n, \\ y_{n+1} = F_2(b, x_n) = bx_n, \end{cases} \tag{1}$$

where a and b are two parameters. This map was originally implemented from the Poincaré section of the Lorenz system, as an example of the sensitivity to the initial conditions in case of weather prediction. To enhance the dynamics of the 2D Hénon map, few researches have been reported to increase its dimension, which yields to the 3D Hénon map [14]

$$\begin{cases} x_{n+1} = c - x_n^2 - dz_n, \\ y_{n+1} = x_n, \\ z_{n+1} = y_n. \end{cases} \tag{2}$$

Fig. 2(a) and (b) depict the Lyapunov exponents of the 2D Hénon map (1) and the 3D Hénon map (2) with the parameters $a \in [0, 1.42]$, $b = 0.3$ and $c \in [0, 1.77]$, $d = 0.1$, respectively. It can be seen that the chaotic behavior of the 2D Hénon map is very limited and occurred only when $a \in [1.05, 1.22] \cup [1.25, 1.42]$, and this map has no hyperchaotic behavior. Whereas, the 3D Hénon map has hyperchaotic behavior, but this behavior is appeared only when $c \in [1.48, 1.79]$. Additionally, the chaotic attractors of the 2D Hénon map and the 3D Hénon map are plotted by setting the parameters $a = 1.4$, $b = 0.4$, $c = 1.5$ and $d = 0.1$, as illustrated in Fig. 2(c) and (d), respectively. It can be observed from Fig. 2(c) and (d) that the 2D and 3D Hénon maps occupy a small region in their phase space. Therefore, enhancing chaotic behaviors of such discrete chaotic systems can significantly encourage the research of chaos sensors applications.

2.1. Chaotifying the 2D Hénon map

To enhance the sensitivity of discrete chaotic systems, we present a cosine chaotification technique and apply it on the 2D Hénon map. Thus, it can be called as chaotifying Hénon map (CHM). The proposed CHM is designed by using a cosine function as a nonlinear transform to enhance the chaotic behavior of the Eq. (1), hence a new 2D hyperchaotic map is obtained. Fig. 3 shows the mechanism that uses to establish the new hyperchaotic map, in which the 2D Hénon map is used to feed the input of the cosine function, and then the result is scaled by a factor of δ. Thus, the new 2D hyperchaotic

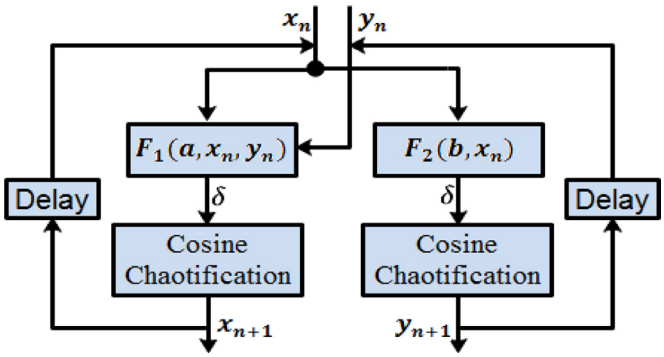

Fig. 3. The structure of chaotifying Hénon map.

map is defined by the following difference equations

$$\begin{cases} x_{n+1} = \delta \cos\left(1 - \alpha x_n^2 + y_n\right), \\ y_{n+1} = \delta \cos\left(\beta x_n\right), \end{cases} \tag{3}$$

where δ, α and β are parameters.

2.2. Equilibrium points and stability

An equilibrium point q of a function $f(x)$ is an element in the domain of $f(x)$, in which it can map itself by $f(x)$. In another word, q is an equilibrium point of the function $f(x)$ only when $f^n(q) = q$. Therefore, the equilibrium points of the system (3) can calculated by solving the following two equations

$$\begin{cases} x^{(v)} = \delta \cos\left(1 - \alpha (x^{(v)})^2 + y^{(v)}\right), \\ y^{(v)} = \delta \cos\left(\beta x^{(v)}\right), \end{cases} \tag{4}$$

where $(v = \mp 1, \mp 2, \ldots, \mp M)$. Eq. (4) can be reduced to the 1D map as follows

$$x^{(v)} = \delta \cos\left(1 - \alpha (x^{(v)})^2 + \delta \cos\left(\beta x^{(v)}\right)\right). \tag{5}$$

The distribution of the elements $x^{(v)}$ can be found by means of a geometric technique, as shown in Fig. 4. In this figure, the distributions of $x^{(v)}$ of Eq. (5) are plotted with fixing the parameter $\alpha = 0.5$ and for different values of parameters δ and β. Meanwhile, the elements $y^{(v)}$ are dependent on the calculated values of $x^{(v)}$, and those can be found by the second equation of Eq. (4). It is obvious that the system (3) has different number of equilibrium points, and the number of these equilibria is dependent on the values of parameters δ and β, in which the number of equilibria are increased whenever the parameters δ and β increase.

The stability of equilibrium points $P^{(v)}(x^{(v)}, y^{(v)})$ can be analyzed by calculating the Jacobian matrix of the system (3), which is given by

$$J = \begin{pmatrix} \frac{\partial x_{n+1}}{\partial x_n} & \frac{\partial x_{n+1}}{\partial y_n} \\ \frac{\partial y_{n+1}}{\partial x_n} & \frac{\partial y_{n+1}}{\partial y_n} \end{pmatrix},$$

that yields

$$J_{P^{(v)}} = \begin{pmatrix} 2\alpha\delta x^{(v)} \sin\left(1 - \alpha (x^{(v)})^2 + y^{(v)}\right) & -\delta \sin\left(1 - \alpha (x^{(v)})^2 + y^{(v)}\right) \\ -\beta\delta \sin(\beta x^{(v)}) & 0 \end{pmatrix},$$

and then finding the corresponding characteristic equation, which is given by

$$\lambda^2 - \phi_1 \lambda - \phi_2 \cdot \phi_3 = 0,$$

where ϕ_1, ϕ_2 and ϕ_3 are defined as

$$\begin{cases} \phi_1 = 2\alpha\delta x^{(v)} \sin\left(1 - \alpha (x^{(v)})^2 + y^{(v)}\right), \\ \phi_2 = \delta \sin\left(1 - \alpha (x^{(v)})^2 + y^{(v)}\right), \\ \phi_3 = \beta\delta \sin(\beta x^{(v)}). \end{cases}$$

Thus, one can obtain

$$\lambda_{1,2} = \frac{\phi_1 \pm \sqrt{\phi_1^2 + 4\phi_2\phi_3}}{2}$$

Table 1
The equilibrium points of the system (3) and their stability with $\alpha = 0.5$.

Parameters	Equilibrium points	λ_1	λ_2	Figure
$\delta = 1,\ \beta = 1$	$P^{(-1)}(-0.3209, 0.9490)$	$-0.1520 + 0.5250i$	$-0.1520 - 0.5250i$	Fig. 4(a)
	$P^{(2)}(1.6678, -0.1937)$	$-0.9202 + 1.1618i$	$-0.9202 - 1.1618i$	
$\delta = 2,\ \beta = 1$	$P^{(1)}(1.2315, 0.6656)$	2.9484	-1.0079	Fig. 4(b)
	$P^{(-1)}(-0.8323, 1.3464)$	$-0.7568 + 1.4549i$	$-0.7568 - 1.4549i$	
	$P^{(2)}(1.7228, -0.4240)$	$-1.9013 + 1.5792i$	$-1.9013 - 1.5792i$	
	$P^{(1)}(1.2482, 0.8877)$	4.5812	-1.4528	
$\delta = 2.8,\ \beta = 1$	$P^{(-1)}(-1.0204, 1.4645)$	$-1.3303 + 2.1102i$	$-1.3303 - 2.1102i$	Fig. 4(c)
	$P^{(-2)}(-2.050, -1.2910)$	4.8808	-0.9709	
	$P^{(-3)}(-2.3475, -1.9626)$	-1.3903	-2.1920	

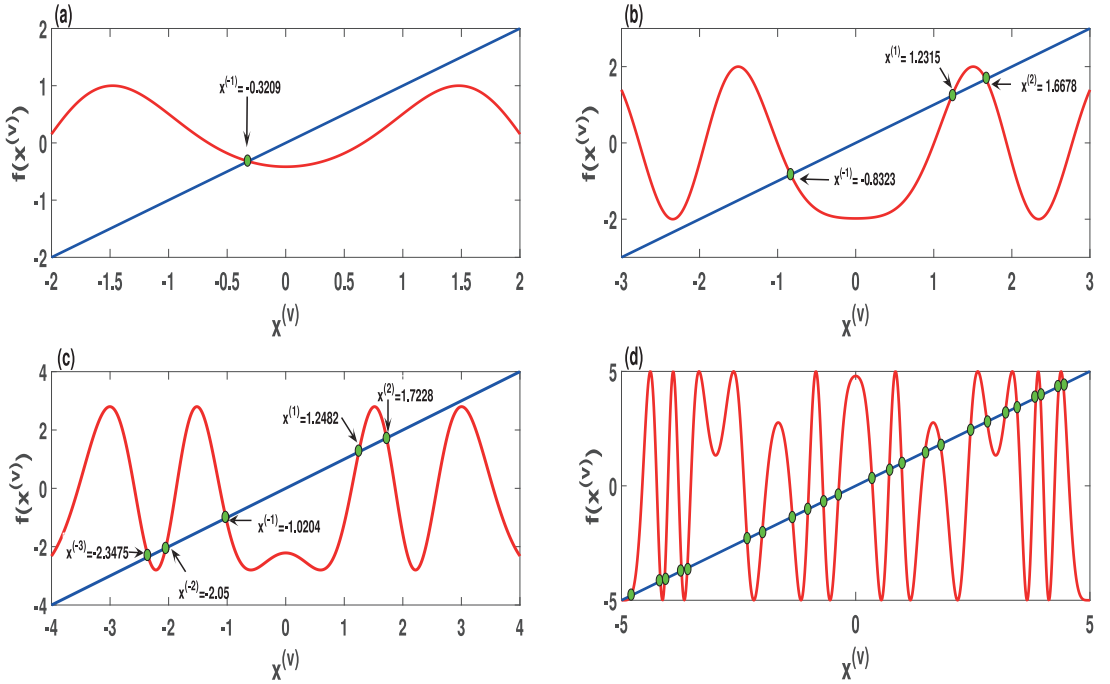

Fig. 4. Equilibrium points $x^{(v)}$ of the system (3) when $\alpha = 0.5$ for the initial values (0.1, 0.1) and with the parameters: (a) $\delta = 1$ and $\beta = 1$; (b) $\delta = 2$ and $\beta = 1$; (c) $\delta = 2.8$ and $\beta = 1$; (d) $\delta = 5$ and $\beta = 3$.

However, the equilibrium points of the system (3), which are appeared in Fig. 4, are listed in Table 1 with their corresponding stability analysis.

3. Dynamics and complexity performance

This section investigates the time series complexity as well as the complicated hyperchaotic behavior of the new 2D discrete system (3) by means of chaotic attractor, Lyapunov exponent, and Sample entropy.

3.1. Chaotic attractor

In discrete chaotic systems, the attractor is a series of discrete values that describes the system motion. Typically, the chaotic attractor occupies an area of the phase plane, and this area can demonstrate the randomness of the system.

Fig. 5(a)–(d) show the chaotic attractors of the system (3) with $\alpha = 0.1$ and different values of parameters δ and β, in which the δ equal to 3, 5 and β equal to 0.5, 0.7, 5 for the initial values (0.1, 0.1). In our experiment, we choose the iteration points to be from 5, 000 to 100, 000 with a view to have an actual chaotic orbit. It can be observed from Fig. 5 that the chaotic attractors of the system (3) occupy a larger region in the phase plane and the series of values spreads more uniformly whenever the parameters values of δ and β are increased. Therefore, it can be concluded that the system (3) has more random output sequences compared with the 2D and 3D Hénon maps.

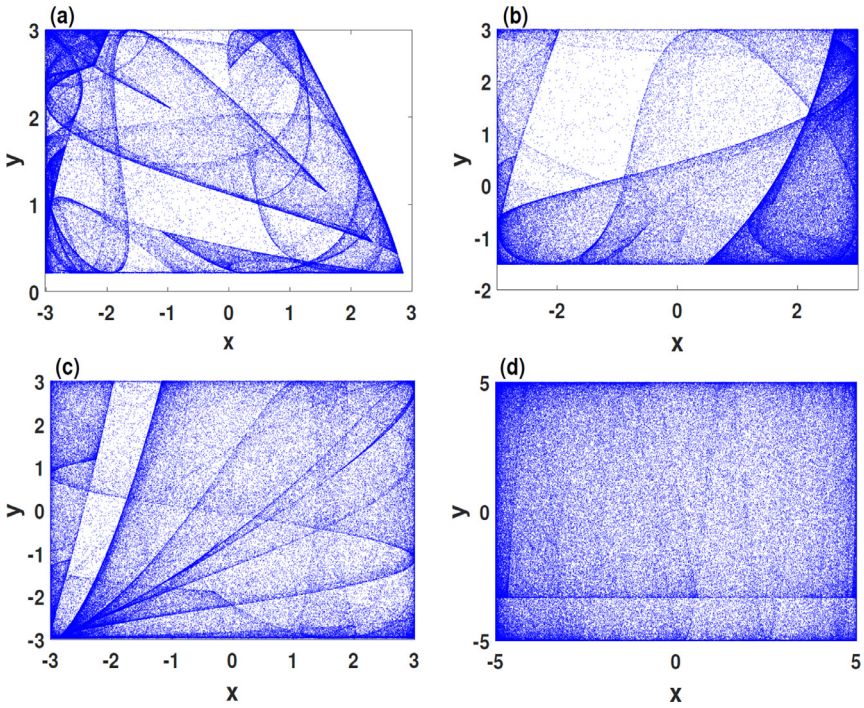

Fig. 5. Chaotic attractor of the system (3) for the initial values (0.1, 0.1) and with $\alpha = 0.1$: (a) $\delta = 3$ and $\beta = 0.5$; (b) $\delta = 3$ and $\beta = 0.7$; (c) $\delta = 3$ and $\beta = 1$; (d) $\delta = 5$ and $\beta = 5$.

3.2. Chaotic and hyperchaotic behaviors

Lyapunov exponent (LE) indicates to the behavior of a nonlinear dynamical system, in which a system is chaotic if there is at least one positive value of LE and hyperchaotic when there are more than one positive value of LE. The LE of the system (3) can be quantitatively measured by applying the QR decomposition algorithm [34], which is given by

$$\begin{aligned} qr[J_M J_{M-1} \dots J_1] &= qr[J_M J_{M-1} \dots J_2 (J_1 Q_0)] \\ &= qr[J_M J_{M-1} \dots J_3 (J_2 Q_1)][R_1] \\ &= qr[J_M J_{M-1} \dots J_i (J_{i-1} Q_{i-2})][R_{i-1} \dots R_1] \\ &= \dots \\ Q_M[R_M \dots R_2 R_1] &= Q_M R \end{aligned}$$

Here, J represents the Jacobian matrix of the system (3), and qr[·] is the QR decomposition function. Consequently, the LE can be obtained by

$$LE = \frac{1}{N} \sum_{i=1}^{N} \ln \mid R_i(v, v) \mid$$

where $v = 1, 2, \dots$ and N is the iteration number.

To prove the complicated chaotic behavior of the system (3), Fig. 6(a) plots its LE for the initial values (0.1, 0.1) with $\delta = 6$, $\alpha = 0.5$ and the parameter β varying from 1.5 to 20. It can be observed from Fig. 6(a) that the system (3) is overall hyperchaotic, and it has much wider chaotic and hyperchaotic behaviors than the 2D and 3D Hénon maps. In addition, the dynamical behaviors of the system (3) is studied in a broad region when two parameters varying simultaneously, as shown in Fig. 6(b) and (c). In Fig. 6(a) and (b), the largest LE (λ_1) and the smallest LE (λ_2) based contour plots are depicted when $\alpha = 0.5$ and δ, $\beta \in [1, 8]$, respectively. Obviously, the system (3) exhibits non-chaotic behaviors only in the yellow, green and blue regions; otherwise it shows the hyperchaotic behavior.

3.3. Complexity performance

The complexity of time series of chaotic systems has attracted attention in recent years because of its importance to measure the predictability of systems. Many algorithms can be applied to measure the complexity of dynamical systems

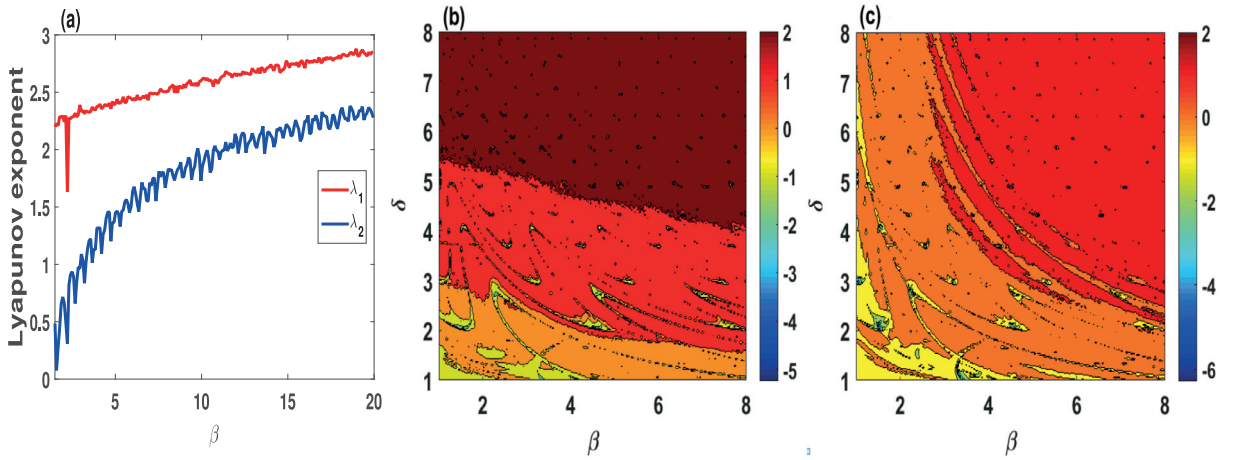

Fig. 6. Lyapunov exponent (LE) analysis of the system (3) for the initial values (0.1, 0.1): (a) LE with $\delta = 6$, $\alpha = 0.5$ and $\beta \in [1.5, 20]$; (b) and (c) Largest and Lowest LE-based contour plots in the $\beta - \delta$ parameters plane with $\alpha = 0.5$, respectively (For interpretation of the references to color in this figure legend, the reader is referred to the web version of this article.).

such as approximate entropy [35], permutation entropy [36], fuzzy entropy [37]. However, we use Sample Entropy (SamEn) [38] in our experiments due to its simplicity, robustness and fast calculation.

Suppose that the time series $(x_i, i = 0, 1, 2, \ldots, N-1)$ with a length of N, SamEn algorithm is calculated according to the following four steps.

1. Phase-space reconstruction: for a given embedding dimension m and time delay τ, the reconstruction sequences are given by

$$X_i = \{x_i, x_{i+\tau}, \ldots, x_{i+(m-1)\tau}\}, \quad X_i \in R^m \tag{6}$$

where $i = 1, 2, \ldots, N - m + \tau$.

2. Counting the vector pairs: let B_i be the number of vector X_j such that

$$d[X_i, X_j] \leq r, \quad i \neq j \tag{7}$$

where r is the tolerance parameter, and $d[X_i, X_j]$ is the distance between X_i and X_j, which is defined as

$$d[X_i, X_j] = max\{|x(i+k) - x(j+k)| : 0 \leq k \leq m-1\}. \tag{8}$$

3. Calculating probability: according to the obtained number of vector pairs, we can get

$$C_i^m(r) = \frac{B_i}{N - (m-1)\tau}, \tag{9}$$

then calculate the probability by

$$\theta^m(r) = \frac{\sum_{i=1}^{N-(m-1)\tau} lnC_i^m(r)}{[N - (m-1)\tau]} \tag{10}$$

4. Calculating SamEn: repeating the above steps we can get $\theta^{m+1}(r)$, then SamEn is given by

$$SamEn(m, r, N) = \theta^m(r) - \theta^{m+1}(r). \tag{11}$$

To examine the complexity of the system (3), the contour plot of SamEn is employed for the embedding dimension $m = 2$ and tolerance parameter $r = 0.2 \times SD$, and the results are illustrated in Fig. 7. Fig. 7(a) and (b) exhibit the complexity of the system (3) when δ and β are varied from 1 to 6 with α equal to 0.5 and 0.9, respectively. It can be observed that SamEn results agree with the LE and chaotic attractor, in which the system (3) has better complexity whenever its parameters increase. Moreover, Fig. 8 depicts the visualization comparison of the time series complexity of the system (3), the 2D Hénon map and the 3D Hénon map when their parameters α, a, c varying. Obviously, the system (3) has much better complexity performance than the other two chaotic maps, which means that its output is much difficult to be predicted.

4. Sensitivity analysis

The Sensitivity on initial condition and parameters is one of essential characteristics of chaotic systems, in which a tiny error in an initial condition or a control parameter can significantly increase in each iteration. However, many existing chaotic systems have low sensitivity, hence this can reduce their role in chaos-based sensor applications. Therefore, it is crucial to enhance the sensitivity of existing chaotic system to be suitable for such applications.

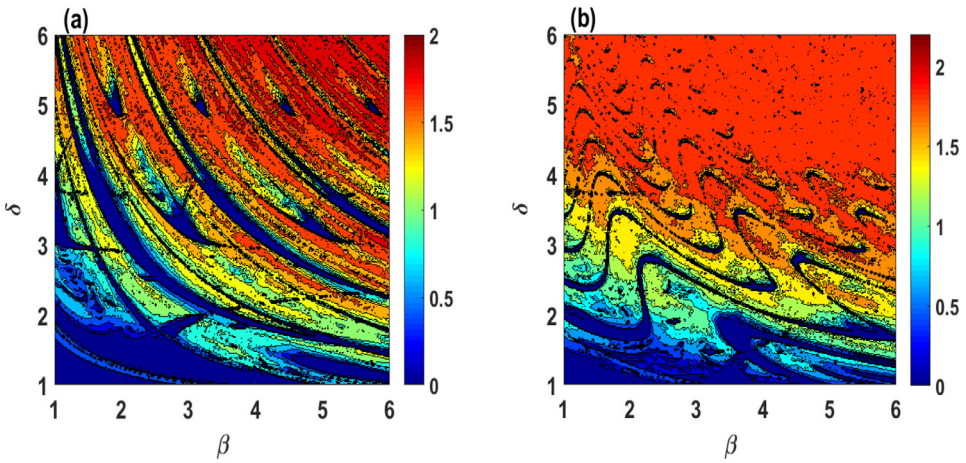

Fig. 7. SamEn-based contour plots in the $\beta - \delta$ parameters plane for the initial values (0.1, 0.1): (a) $\alpha = 0.5$; (b) $\alpha = 0.9$.

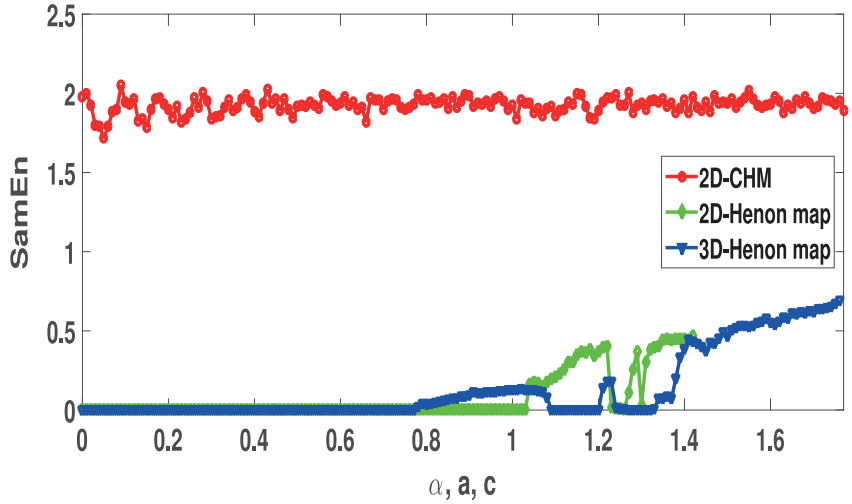

Fig. 8. SamEn results comparison of the 2D-CHM, 2D Hénon map, and 3D Hénon map for the initial values $(x_0, y_0) = (0.1, 0.1)$ and $(x_0, y_0, z_0) = (0.1, 0.1, 0.1)$ with the parameters $\delta = 6$, $\beta = 5$, $b = 0.3$, $d = 0.1$, and α, a, $c \in [0, 1.77]$.

4.1. Cross-correlation coefficient

To estimate the sensitivity of the time series of the system (3), 2D Hénon map and 3D Hénon map, we use the cross-correlation coefficient (CCF), which is given by

$$CCF(A_t, B_t) = \frac{\sum_{t=1}^{N}(A_t - m(A))(B_t - m(B))}{\sqrt{\sum_{t=1}^{N}(A_t - m(A))^2 \sum_{t=1}^{N}(B - m(B))^2}}, \tag{12}$$

where $m(A)$ and $m(B)$ are the mean values of the two time series A_t and B_t, respectively. The two time series A_t and B_t are diverged from each other if $CCF(A_t, B_t)$ is converged to 0, whereas, A_t and B_t are converged to each other if $CCF(A_t, B_t)$ is converged to 1.

The sensitivity of time series of the system (3), 2D Hénon map and 3D Hénon map are illustrated in Fig. 9. The first column of Fig. 9 plot the CCF between the nominal time series T_1 and the new time series $(T_2 = T_1 + e)$, which is obtained by adding a tiny error $e = 5 \times 10^{-15}$ to the initial values of the three chaotic maps. Meanwhile, the second column of Fig. 9 depict the CCF between T_1 and the new time series $(T_3 = T_1 + e)$, which is obtained by adding e to the parameters of these chaotic maps. In our experiments, we examine only the chaotic regions of these chaotic maps, hence we set the parameters $a \in [1.25, 1.42]$, $b = 0.3$, $c \in [1.45, 1.77]$, $d = 0.1$, $\delta = \beta = 7$, and $\alpha \in [0.1, 1]$ with the initial conditions (0.1, 0.1) for the 2D maps and (0.1, 0.1, 0.1) for the 3D map. Obviously, the system (3) is very sensitive to its initial condition and parameters, and also has higher sensitivity than the other two chaotic maps.

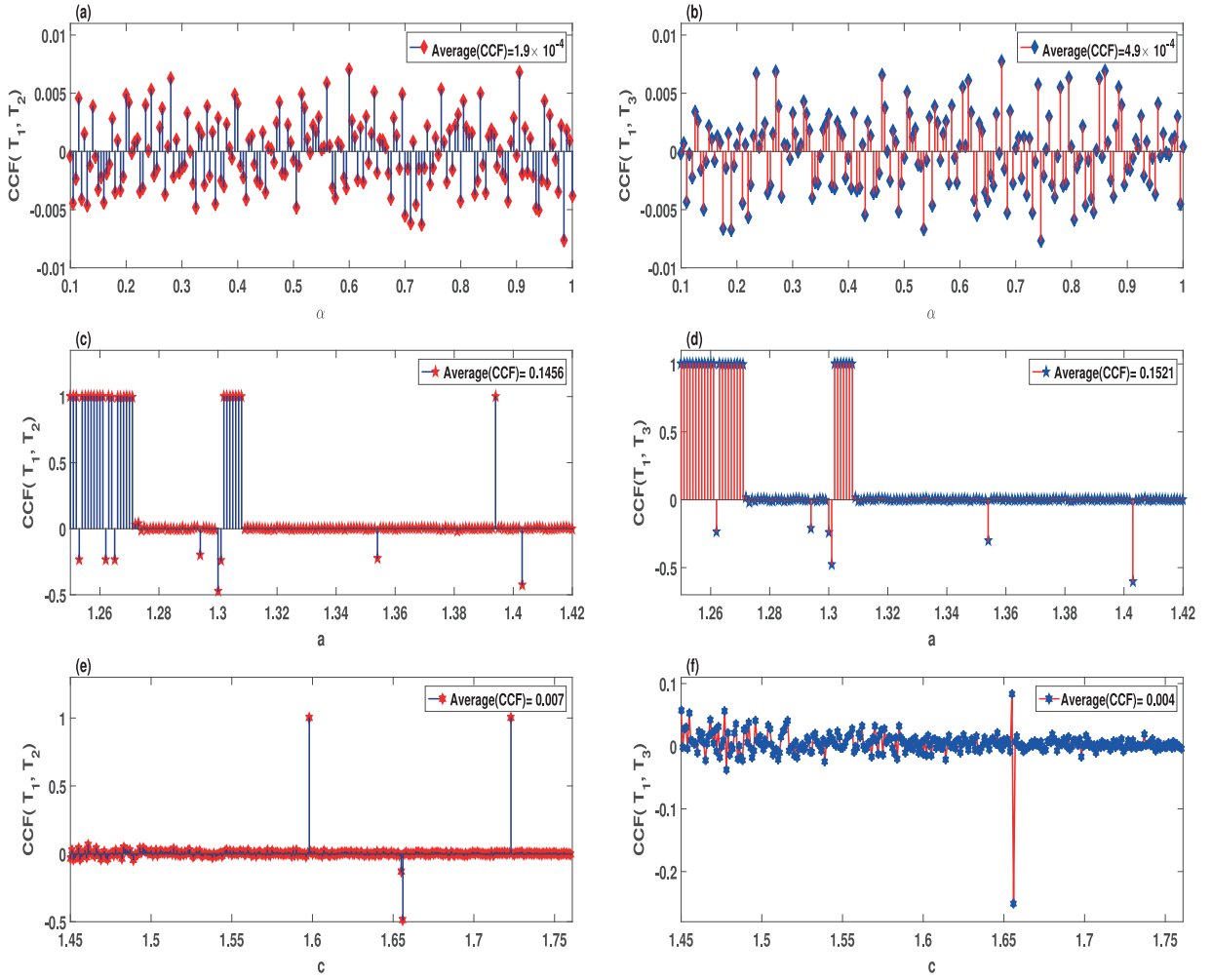

Fig. 9. Cross-correlation coefficient (CCF) analysis: (a) the CCF of the system (3) with $\delta = \beta = 7$, and $\alpha \in [0.1, 1]$ for the initial values $(0.1 + e, 0.1)$; (b) the CCF of the system (3) with $\delta = 7 + e$, $\beta = 7$ and $\alpha \in [0.1, 1]$ for the initial values (0.1, 0.1); (c) the CCF of the 2D Hénon map with $a \in [1.25, 1.42]$ and $b = 0.3$ and for the initial values $(0.1 + e, 0.1)$; (d) the CCF of the 2D Hénon map with $a \in [1.25, 1.42]$ and $b = 0.3 + e$ and for the initial values (0.1, 0.1); (e) the CCF of the 3D Hénon map with $c \in [1.45, 1.77]$ and $d = 0.1$ and for the initial values $(0.1 + e, 0.1)$; (f) the CCF of the 3D Hénon map with $c \in [1.45, 1.77]$ and $d = 0.1 + e$ and for the initial values (0.1, 0.1).

4.2. The number of non-divergent trajectories

In chaotic systems, any two close trajectories with different initial conditions are either diverged or converged from each other in each iteration. Therefore, a chaotic system is more sensitive to its initial condition when the close trajectories are diverged in each iteration as much as possible. To test the sensitive of the system (3), 2D Hénon map and 3D Hénon map for a specific number of iterations, we designed the following experiment for each chaotic map: (1) choose the parameters of the map that show chaotic behaviors; (2) find a time series S_1 with length 100, 000 for the initial values I_1; (3) select an another initial values I_2, which is neighbor to I_1, by adding a small value k to I_1; (4) obtain a time series S_2 with length 100, 000 for the initial values I_2; (5) calculate the number of non-divergent trajectories (NDT), which is defined by

$$NDT = \sum_{i=1}^{M} | S_{1i} - S_{2i} | \leq k, \tag{13}$$

where $M = 100,000$. Fig. 10(a) describes the mechanism of how the sensitivity test is worked out. To show the sensitivity of the system (3), 2D Hénon map and 3D Hénon map, Fig. 10(b)–(d) plot their NDT with different values of k, respectively. It is clear that the NDT of the system (3) is less than the NDT of the other two chaotic maps, hence the system (3) is more sensitive to its initial conditions.

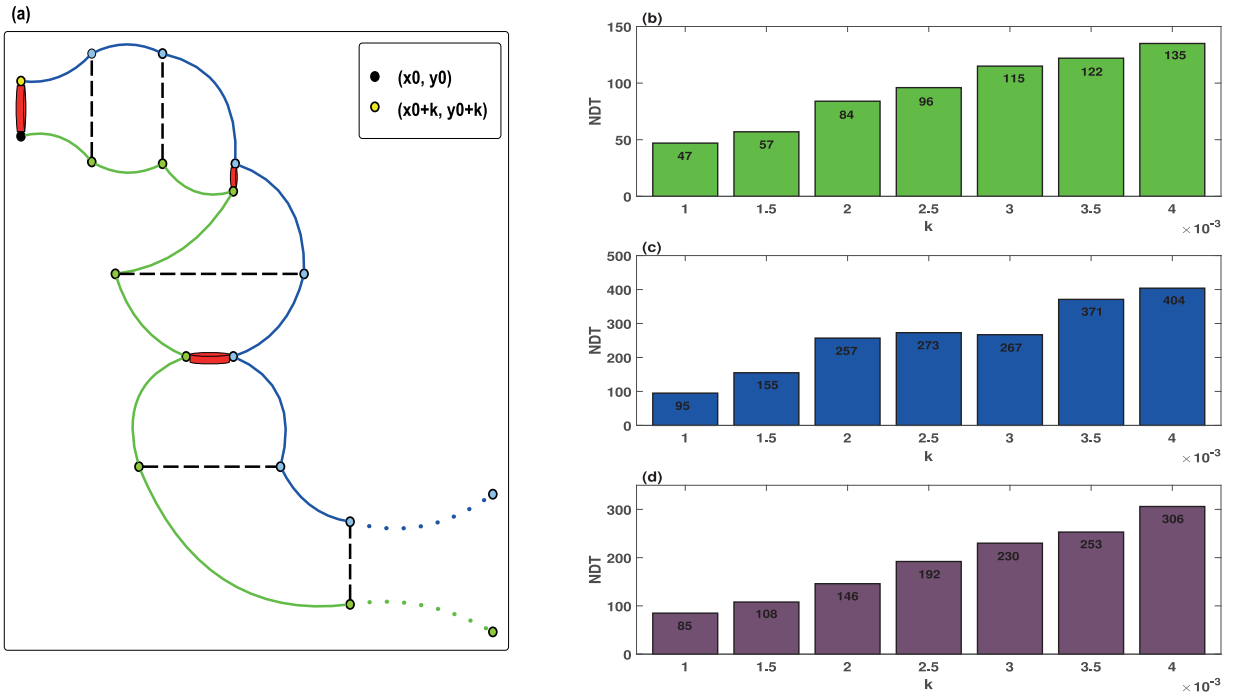

Fig. 10. The number of non-divergent trajectories (NDT) for the initial values $(0.1+k, 0.1)$ and $(0.1+k, 0.1, 0.1)$, where $k \geq 0$; (a) the mechanism of how the NDT is worked out; (b), (c), (d) the NDT of the system (3), 2D Hénon map, and 3D Hénon map, respectively, when their parameters are set as $\delta = 6$, $\alpha = 0.5$, $\beta = 8$, $a = 1.4$, $b = 0.3$, $c = 1.76$, and $d = 0.1$.

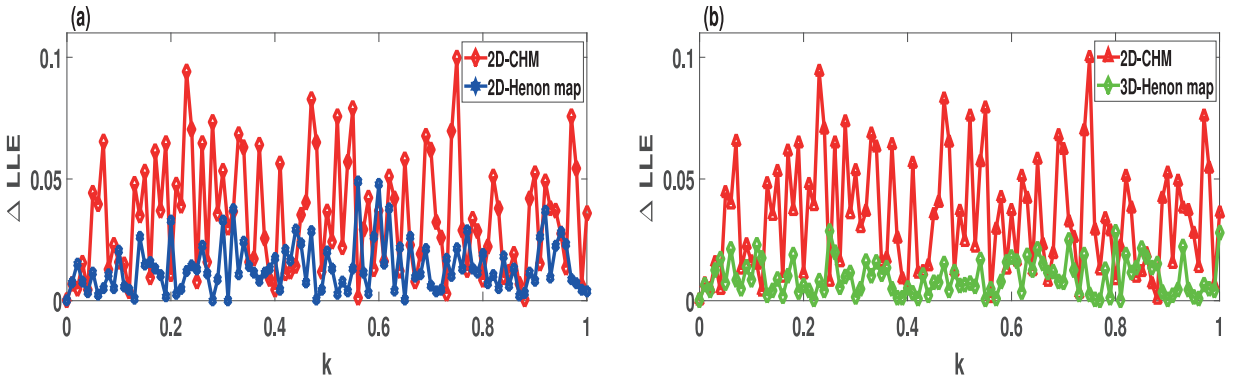

Fig. 11. Change of the largest LE comparison for the initial values $(0.1+k, 0.1)$ and $(0.1+k, 0.1, 0.1)$, where $k \geq 0$; (a) the change of complexity of the systems (3) and the 2D Hénon map with the parameters $\delta = 8$, $\alpha = 0.5$, $\beta = 8$, $a = 1.4$, and $b = 0.3$; (b) the change of complexity of the systems (3) and the 3D Hénon map with the parameters $\delta = 8$, $\alpha = 0.5$, $\beta = 8$, $c = 1.77$, and $d = 0.1$.

4.3. Change of complexity

Although the Largest Lyapunov exponents (LLE) cannot detect if a chaotic system is hyperchaotic or not, it is an important measure for evaluating the complexity of chaotic systems. However, the LLE of a sensitive chaotic system should be changed with any small error to the initial condition of the system. To investigate how much the change in the complexity of the system (3), 2D Hénon map and 3D Hénon map, Fig. 11 depicts the difference between the LLE of these chaotic maps for a give set of initial condition (x_0, y_0) or (x_0, y_0, z_0) and the LLE of same chaotic maps, but with the initial condition $(x_0 + k, y_0)$ or $(x_0 + k, y_0, z_0)$. It is obvious that the change of complexity of the system (3) is much higher than the change of the 2D Hénon map and 3D Hénon map, which means that it is more sensitive than the other two chaotic maps.

4.4. Possible implementations

The 2D and 3D Hénon maps are the prototypes to establish our novel proposed features. We choose discrete models since those models are effective for communications as well as implementing pseudo random number sequences (PRNS). Furthermore, several communication, optical, environmental models with sensing features can be approximated with discrete dynamics. In fact, the basic implementations of the proposed theory towards IoT is simple. The chaotic models can be easily implementation with analog or digital circuits, and also FPGA implementations [39]. The 2D and 3D maps are the simple models to have successful enhancement of sensitivity. More complicated models can also be used and effective with FPGA implementations [40].

Moreover, complexity plays an important role to quantify the amount of uncertainty inside the dynamics. In the emerging world of IoT and the vast area of nonlinear dynamics, complexity can be considered as a bridge of connections. We have shown that the sensitivity of a chaos sensor is proportional to the dynamical complexity. Dynamical complexity is considered as the fundamental and essential concept in information theory. Several entropy measures are available to quantify complexity. Apart from that Lyapunov exponents, fractal dimensions, visual recurrence analysis etc are usually used to describe the uncertainty of chaotic systems. The implementation can be done using several circuits as researchers are effectively implementing in Information Theory. For example, in case of optical sensor, one can implement optical complexity, which has been investigated as a well applied tool and a metric proportional to the Intensity of the lasers [20].

5. Conclusion

This paper proposed the cosine chaotification technique to enhance the chaotic characteristics of discrete systems such as sensitivity, randomness, and complexity. As a typical example, this technique applied on the 2D Hénon map. The dynamical analysis have shown that the enhanced Hénon map can have different number of equilibria. The chaotic characteristics evaluations including Lyapunov exponent, chaotic attractor, sensitivity, and complexity have demonstrated that the enhanced Hénon map has large hyperchaotic regions, high complexity and sensitivity to its initial values and parameters. Therefore, the enhanced Hénon map have achieved the major requirements of chaos-based sensor applications.

Declaration of interests

The authors declare that they have no known competing financial interests or personal relationships that could have appeared to influence the work reported in this paper.

References

[1] V.G. Ivancevic, T.T. Ivancevic, Complex Nonlinearity: Chaos, Phase Transitions, Topology Change and Path Integrals, Springer Science & Business Media, 2008.
[2] S. Banerjee, P. Saha, A.R. Chowdhury, Chaotic aspects of lasers with host-induced nonlinearity and its control, Phys. Lett. A 291 (2–3) (2001) 103–114.
[3] H. Natiq, S. Banerjee, A. Misra, M. Said, Degenerating the butterfly attractor in a plasma perturbation model using nonlinear controllers, Chaos Solit. Fract. 122 (2019) 58–68.
[4] P. Mukherjee, S. Banerjee, Projective and hybrid projective synchronization for the Lorenz–stenflo system with estimation of unknown parameters, Phys. Scripta 82 (5) (2010) 055010.
[5] D. Yu, F. Liu, P.-Y. Lai, Input reconstruction of chaos sensors, Chaos Interdiscipl. J. Nonlinear Sci. 18 (2) (2008) 023106.
[6] S. Banerjee, P. Saha, A.R. Chowdhury, Optically injected laser system: characterization of chaos, bifurcation, and control, Chaos Interdiscipl. J. Nonlinear Sci. 14 (2) (2004) 347–357.
[7] S. Banerjee, S. Jeeva Sathya Theesar, J. Kurths, Generalized variable projective synchronization of time delayed systems, Chaos Interdiscipl. J. Nonlinear Sci. 23 (1) (2013) 013118.
[8] H. Natiq, N. Al-Saidi, M. Said, A. Kilicman, A new hyperchaotic map and its application for image encryption, Eur. Phys. J. Plus 133 (1) (2018) 6.
[9] H. Natiq, S. Banerjee, S. He, M. Said, A. Kilicman, Designing an m-dimensional nonlinear model for producing hyperchaos, Chaos Solit. Fract. 114 (2018) 506–515.
[10] B. Vaseghi, M.A. Pourmina, S. Mobayen, Secure communication in wireless sensor networks based on chaos synchronization using adaptive sliding mode control, Nonlinear Dyn. 89 (3) (2017) 1689–1704.
[11] L.J. Fiderer, D. Braun, Quantum metrology with quantum-chaotic sensors, Nature Commun. 9 (1) (2018) 1351.
[12] D. Rontani, D. Choi, C.-Y. Chang, A. Locquet, D. Citrin, Compressive sensing with optical chaos, Sci. Rep. 6 (2016) 35206.
[13] M. Hénon, A two-dimensional mapping with a strange attractor, in: The Theory of Chaotic Attractors, Springer, 1976, pp. 94–102.
[14] G. Baier, M. Klein, Maximum hyperchaos in generalized Hénon maps, Phys. Lett. A 151 (1990) 281–284.
[15] E.N. Lorenz, Deterministic nonperiodic flow, J. Atmosph. Sci. 20 (2) (1963) 130–141.
[16] O.E. Rössler, An equation for continuous chaos, Phys. Lett. A 57 (5) (1976) 397–398.
[17] J.C. Sprott, Some simple chaotic flows, Phys. Rev. E 50 (2) (1994) R647.
[18] J. Lü, G. Chen, A new chaotic attractor coined, Int. J. Bifurcat. Chaos 12 (03) (2002) 659–661.
[19] S. He, K. Sun, S. Banerjee, Dynamical properties and complexity in fractional-order diffusionless lorenz system, Eur. Phys. J. Plus 131 (8) (2016) 254.
[20] L. Rondoni, M. Ariffin, R. Varatharajoo, S. Mukherjee, S.K. Palit, S. Banerjee, Optical complexity in external cavity semiconductor laser, Optics Commun. 387 (2017) 257–266.
[21] H. Natiq, S. Banerjee, M. Ariffin, M. Said, Can hyperchaotic maps with high complexity produce multistability? Chaos Interdiscipl. J. Nonlinear Sci. 29 (1) (2019) 011103.
[22] H. Natiq, M. Said, M. Ariffin, S. He, L. Rondoni, S. Banerjee, Self-excited and hidden attractors in a novel chaotic system with complicated multistability, Eur. Phys. J. Plus 133 (12) (2018) 557.
[23] H. Natiq, M. Said, N. Al-Saidi, A. Kilicman, Dynamics and complexity of a new 4d chaotic laser system, Entropy 21 (1) (2019) 34.
[24] Z. Hua, B. Zhou, Y. Zhou, Sine-transform-based chaotic system with FPGA implementation, IEEE Trans. Ind. Electron. 65 (3) (2018) 2557–2566.
[25] Z. Hua, Y. Zhou, C.-M. Pun, C.P. Chen, 2d sine logistic modulation map for image encryption, Inf. Sci. 297 (2015) 80–94.
[26] Y. Zhou, Z. Hua, C.-M. Pun, C.P. Chen, Cascade chaotic system with applications, IEEE Trans. Cybern. 45 (9) (2015) 2001–2012.

[27] Z. Hua, Y. Zhou, Dynamic parameter-control chaotic system., IEEE Trans. Cybern. 46 (12) (2016) 3330–3341.
[28] H. Natiq, S. Banerjee, M. Said, Cosine chaotification technique to enhance chaos and complexity of discrete systems, Eur. Phys. J. Special Topics 228 (1) (2019) 185–194.
[29] R. Gorrepotu, N.S. Korivi, K. Chandu, S. Deb, Sub-1ghz miniature wireless sensor node for IoT applications, Internet Things 1 (2018) 27–39.
[30] E.G. Petrakis, S. Sotiriadis, T. Soultanopoulos, P.T. Renta, R. Buyya, N. Bessis, Internet of things as a service (itaas): challenges and solutions for management of sensor data on the cloud and the fog, Int. Things 3 (2018) 156–174.
[31] A. Ohnishi, K. Murao, T. Terada, M. Tsukamoto, A method for structuring meeting logs using wearable sensors, Int. Things 5 (2019) 140–152.
[32] H. Suo, J. Wan, C. Zou, J. Liu, Security in the internet of things: a review, in: Proceedings of the International Conference on Computer Science and Electronics Engineering (ICCSEE), 3, IEEE, 2012, pp. 648–651.
[33] M. Hasan, M.M. Islam, M.I.I. Zarif, M. Hashem, Attack and anomaly detection in IoT sensors in IoT sites using machine learning approaches, Int. Things 7 (2019) 100059.
[34] F. Hubertus, F.E. Udwadia, W. Proskurowski, An efficient QR based method for the computation of Lyapunov exponents, Phys. D 101 (1) (1997) 1–16.
[35] S.M. Pincus, Approximate entropy as a measure of system complexity., Proc. Natl. Acad. Sci. 88 (6) (1991) 2297–2301.
[36] C. Bandt, B. Pompe, Permutation entropy: a natural complexity measure for time series, Phys. Rev. Lett. 88 (17) (2002) 174102.
[37] C. Liu, K. Li, L. Zhao, F. Liu, D. Zheng, C. Liu, S. Liu, Analysis of heart rate variability using fuzzy measure entropy, Comput. Biol. Med. 43 (2) (2013) 100–108.
[38] J.S. Richman, J.R. Moorman, Physiological time-series analysis using approximate entropy and sample entropy, Am. J. Physiol. Heart Circul. Physiol. 278 (6) (2000) H2039–H2049.
[39] B. Muthuswamy, S. Banerjee, A Route to Chaos Using FPGAs, Springer, 2015.
[40] D. Valli, B. Muthuswamy, S. Banerjee, M. Ariffin, A. Wahab, K. Ganesan, C. Subramaniam, J. Kurths, Synchronization in coupled Ikeda delay systems, Eur. Phys. J. Spec. Top. 223 (8) (2014) 1465–1479.